Deposition from Wax−Solvent Mixtures under Turbulent Flow: Effects of Shear Rate and Time on Deposit Properties†

ARTICLE *in* ENERGY & FUELS · MARCH 2009

Impact Factor: 2.79 · DOI: 10.1021/ef800591p

Article

Deposition from Wax#Solvent Mixtures under Turbulent Flow: Effects of Shear Rate and Time on Deposit Properties

Ravindra Tiwary, and Anil K. Mehrotra

Energy Fuels, **2009**, 23 (3), 1299-1310• DOI: 10.1021/ef800591p • Publication Date (Web): 04 December 2008

Deposition from Wax−Solvent Mixtures under Turbulent Flow: Effects of Shear Rate and Time on Deposit Properties†

Ravindra Tiwary and Anil K. Mehrotra*

Department of Chemical and Petroleum Engineering, University of Calgary, Calgary, Alberta T2N 1N4, Canada

Received July 25, 2008. Revised Manuscript Received October 8, 2008

A bench-scale flow-loop apparatus, incorporating a double-pipe heat exchanger, was used for investigating the effects of shear rate and deposition time on the deposition of solids, under turbulent flow, from solutions of a multicomponent wax in a paraffinic solvent. The deposit-layer thickness was found to decrease with an increase in the Reynolds number (or shear rate), while it increased asymptotically with the deposition time. Calculations with a steady-state heat-transfer model showed the liquid−deposit interface temperature to be equal to the wax appearance temperature (WAT) and the deposit average thermal conductivity to be 0.35 W m^{-1} K^{-1}. Gas chromatography (GC) analyses of deposit samples showed significant changes in the carbon number distribution with shear rate and time. A recently proposed model, involving one-dimensional shear deformation of a cubical cage, was used to express changes in the deposit composition, via the deformation angle (β), as a function of the Reynolds number and deposition time. The time-dependent variations in deposit composition were expressed with a viscoplastic model, in which Reynolds number (or shear rate) influences the initial deposit properties. The proposed viscoplastic model affords a new explanation for the deposit aging phenomenon. The deposition from "waxy" mixtures was confirmed to be primarily a thermally driven process, in which the shear rate and deposition time play important roles by influencing the deposit properties.

Introduction

Petroleum crude oils are complex mixtures of numerous hydrocarbons that are divided into different groups, such as alkanes, paraffins, aromatics, naphthenes, resins, asphaltenes, etc. Among these groups of hydrocarbons, high-molecular-weight paraffins are responsible for solids deposition problems encountered during production, transportation, and processing operations in the petroleum industry. When a "waxy" crude oil, comprising high-molecular-weight paraffins, flowing through a pipeline is exposed to a cold environment, i.e., at a temperature below the wax appearance temperature (WAT), solids deposition on the pipe wall is known to occur. The deposition of waxy solids results in plugging of the pipelines, which can cause high pressure drops and increased energy consumption during crude oil transportation.

The highest temperature at which the first crystals of paraffins (waxes) start to appear, upon cooling of a waxy crude oil, is called the WAT. As the crude oil temperature is decreased further below the WAT [but higher than the pour-point temperature (PPT)], wax crystals grow in size and an interlocking network structure is formed, which turns the crude oil into a gel-like structure with entrapped liquid oil. That is, the wax deposit consists of liquid and solid phases. It has been reported that as little as 2% of precipitated wax can be sufficient to form a gel or deposit from a waxy crude oil.[1,2] Recently, Paso et al.[3] reported that low-temperature rheological gels can form from model fluids with *n*-paraffin contents as low as 0.5 wt %. Wax deposition occurs when the pipe surface temperature is below the WAT, and a temperature gradient exits between the crude oil and colder deposition surface. The composition and relative proportions of liquid and solid phases vary across the deposit thickness because of differences in temperature, concentration, and shear rate (because of the flowing oil).

A recent study reported significant difference between the WAT, measured while cooling, and the wax disappearance temperature (WDT), measured while heating.[4] It was shown that the WDT, rather than the WAT, is closer to the thermodynamic liquidus temperature (T_L) of wax−solvent mixtures.[4] That is, WAT < WDT ($\approx T_L$) because of the subcooling associated with the crystallization process.

The deposition from paraffinic mixtures is a complex process, which may involve several considerations, such as the thermodynamics of solid−liquid multiphase equilibria, molecular diffusion or mass transfer, fluid dynamics, heat transfer, rheology, crystallization kinetics, etc. It has been modeled using different approaches, including molecular diffusion, shear dispersion, Brownian diffusion, gravity settling, etc.[5−8] Among these, the molecular diffusion (or concentration gradient) modeling approach has

† Presented at the 9th International Conference on Petroleum Phase Behavior and Fouling.

* To whom correspondence should be addressed. Telephone: (403) 220-7406. Fax: (403) 284-4852. E-mail: mehrotra@ucalgary.ca.

(1) Holder, G. A.; Winkler, J. Wax crystallization from distillate fuels. I. Cloud and pour phenomena exhibited by solutions of binary *n*-paraffin mixtures. *J. Inst. Petrol.* **1965**, *51*, 228.

(2) Singh, P.; Venkatesan, R.; Fogler, H. S.; Nagarajan, N. Formation and aging of incipient thin film wax−oil gels. *AIChE J.* **2000**, *46*, 1059.

(3) Paso, K.; Senra, M.; Yi, Y.; Sastry, A. M.; Fogler, H. S. Paraffin polydispersity facilitates mechanical gelation. *Ind. Eng. Chem. Res.* **2005**, *44*, 7242.

(4) Bhat, N. V.; Mehrotra, A. K. Measurement and prediction of the phase behavior of wax−solvent mixtures: Significance of the wax *dis*appearance temperature. *Ind. Eng. Chem. Res.* **2004**, *43*, 3451.

(5) Burger, E. D.; Perkins, T. K.; Striegler, J. H. Studies of wax deposition in the trans Alaska pipeline. *J. Pet. Technol.* **1981**, *33*, 1075.

(6) Bern, P. A.; Withers, V. R.; Cairns, R. J. R. Wax deposition in crude oil pipelines. European Offshore Petroleum Conference and Exhibition, London, U.K., Oct 21−24, 1980.

10.1021/ef800591p CCC: $40.75
Published on Web 12/04/2008

been used in several studies on wax deposition.[2,5,9−11] The molecular diffusion approach is based on the premise that the deposition is caused by the radial transport of wax molecules, which results from a radial concentration gradient in the liquid phase. In the molecular diffusion approach, the liquid−deposit interface temperature is assumed to increase from an initial value close to the pipe-wall temperature to the WAT at steady state.[2] Within the deposit, the solid−liquid ratio as well as the deposit composition and "hardness" have been observed to vary with time through a process referred to as "deposit aging",[2,10−17] which may be attributed to molecular diffusion within the deposit, the interphase mass transfer, and/or the effect of shear stress or flow rate on the deposit.

Recent studies have identified the importance of heat transfer in the deposition process.[10,14−21] Of particular relevance to this study is the heat-transfer analogy that yielded a good agreement with the experimental results for the deposition of solids from wax−solvent mixtures under laminar as well as turbulent flow.[14−16] The variables affecting the deposit-layer thickness are the oil temperature and flow rate, the pipe-wall temperature, and the wax concentration in the oil. The results from bench-scale tests, conducted over relatively shorter durations of up to 4 h, showed that a smaller deposit-layer thickness can be achieved with a higher oil temperature (i.e., relative to the WAT), a higher flow rate or Reynolds number, a higher pipe-wall temperature (i.e., relative to the WAT), and a lower wax concentration.[13−16] A modeling approach, on the basis of the moving boundary problem formulation, for the formation and growth of the deposit layer from paraffinic mixtures in a pipeline under laminar flow confirmed these experimental observations.[22−24]

Previous wax deposition studies[2,10−21,27−31] under both laminar and turbulent flow conditions with prepared wax−solvent mixtures and "waxy" crude oils have reported that (i) the deposit formation commences soon after the oil is exposed to a wall temperature below the WAT, (ii) the deposit growth continues to occur over time until reaching a constant thickness, (iii) the deposit thickness decreases with an increase in the Reynolds number, the deposit thickness under turbulent flow is much smaller than under laminar flow, (iv) the concentration of heavier paraffins in the deposit increases with time, making the deposit harder, (v) the steady-state liquid−deposit interface temperature, T_d, is equal to the WAT, and (vi) the deposit mass depends upon the individual temperature difference across each of the thermal resistances and not the overall temperature difference.

This study was undertaken to investigate the effects of shear rate and time on deposit properties under turbulent flow conditions. The deposition experiments were performed in a bench-scale apparatus, with heat transfer, using prepared multicomponent wax−solvent mixtures. The experiments were designed to investigate the effects of wax concentration, Reynolds number (or shear rate), and deposition time in the thickness of the deposit layer as well as its composition and properties, such as density and thermal conductivity. Gas chromatography (GC) analyses of deposit samples were used to interpret the changes in the carbon number distribution with shear rate and time. A viscoplastic model was developed to describe the observed increase in the deposit wax content with Reynolds number and deposition time. The results of this study provide further evidence that the deposition from "waxy" mixtures is primarily a thermally driven process, in which the shear rate and the deposition time play important roles by influencing the deposit properties.

Heat-Transfer Calculations

Heat transfer from a "hot" waxy mixture (or crude oil) flowing through a pipe to the "cold" outside environment results in a radial temperature gradient, which would lead to the formation of a deposit layer, provided that the inside pipe-wall temperature is less than the WAT of the "hot" stream. Because of a relatively

(7) Dirand, M.; Chevallier, V.; Provost, E.; Bouroukba, M.; Petitjean, D. Multicomponent paraffin waxes and petroleum solid deposits: Structural and thermodynamic state. *Fuel* **1998**, *77*, 1253.

(8) Azevedo, L. F. A.; Teixeria, A. M. A critical review of the modeling of wax deposition mechanisms. *Pet. Sci. Technol.* **2003**, *21*, 393.

(9) Svendsen, J. A. Mathematical modeling of wax deposition in oil pipeline systems. *AIChE J.* **1993**, *39*, 1377.

(10) Creek, J. L.; Lund, H. J.; Brill, J. P.; Volk, M. Wax deposition in single phase flow. *Fluid Phase Equilib.* **1999**, *158−160*, 801.

(11) Singh, P.; Youyen, A.; Fogler, H. S. Evidence of a critical carbon number in the aging of a wax−oil gel. *AIChE J.* **2001**, *47*, 2111.

(12) Singh, P.; Venkatesan, R.; Fogler, H. S.; Nagarajan, N. Prediction of the wax content of the incipient wax−oil gel in a pipeline: An application of the controlled stress rheometer. *J. Rheol.* **1999**, *43*, 1437.

(13) Coutinho, J. A. P.; Lopes da Silva, J. A.; Ferreira, A.; Soares, M. R.; Daridon, J. L. Evidence for the aging of wax deposits in crude oils by Ostwald ripening. *Pet. Sci. Technol.* **2003**, *21*, 381.

(14) Bidmus, H. O.; Mehrotra, A. K. Heat-transfer analogy for wax deposition from paraffinic mixtures. *Ind. Eng. Chem. Res.* **2004**, *43*, 791.

(15) Parthasarathi, P.; Mehrotra, A. K. Solids deposition from multicomponent wax−solvent mixtures in a benchscale flow-loop apparatus with heat transfer. *Energy Fuels* **2005**, *19*, 1387.

(16) Fong, N.; Mehrotra, A. K. Deposition under turbulent flow of wax−solvent mixtures in a bench-scale flow-loop apparatus with heat transfer. *Energy Fuels* **2007**, *21*, 1263.

(17) Paso, K. G.; Fogler, H. S. Influence of *n*-paraffin composition on the aging of wax−oil gel deposits. *AIChE J.* **2003**, *49*, 3241.

(18) Ghedamu, M.; Watkinson, A. P.; Epstein, N. Mitigation of wax buildup on cooled surfaces. In *Fouling Mitigation of Industrial Heat-Exchange Equipment*; Panchal, C. B., Bott, T. R., Somerscales, E. F. C., Toyama, S., Eds.; Begel House: New York, 1997; pp 473−489.

(19) Cordoba, A. J.; Schall, C. A. Application of a heat transfer method to determine wax deposition in a hydrocarbon binary mixture. *Fuel* **2001**, *80*, 1285.

(20) Bott, T. R.; Gudmunsson, J. S. Deposition of paraffin wax from kerosene in cooled heat exchanger tubes. *Can. J. Chem. Eng.* **1977**, *55*, 381.

(21) Wu, C.; Wang, K. S.; Shuler, P. J.; Tand, Y.; Creek, J. L.; Carlson, R. M.; Cheung, S. Measurement of wax deposition in paraffin solutions. *AIChE J.* **2002**, *48*, 2107.

(22) Bhat, N. V.; Mehrotra, A. K. Modeling of deposit formation from "waxy" mixtures via moving boundary formulation: Radial heat transfer under static and laminar flow conditions. *Ind. Eng. Chem. Res.* **2005**, *44*, 6948.

(23) Bhat, N. V.; Mehrotra, A. K. Modeling of deposition from "waxy" mixtures in a pipeline under laminar flow conditions via moving boundary formulation. *Ind. Eng. Chem. Res.* **2006**, *45*, 8728.

(24) Bhat, N. V.; Mehrotra, A. K. Modeling the effect of shear stress on composition and growth of deposit layer from "waxy" mixtures under laminar flow in a pipeline. *Energy Fuels* **2008**, *22*, 3237.

(25) Tiwary, R. Effects of shear rate and time on deposition from wax−solvent mixtures under turbulent flow. M.Sc. Thesis, University of Calgary, Calgary, Canada, 2008.

(26) Fong, N. An experimental investigation of deposition from wax−solvent mixtures under turbulent flow with heat transfer. M.Sc. Thesis, University of Calgary, Calgary, Canada, 2007.

(27) Mehrotra, A. K.; Bhat, N. V. Modeling the effect of shear stress on deposition from "waxy" mixtures under laminar flow with heat transfer. *Energy Fuels* **2007**, *21*, 1277.

(28) Bidmus, H.; Mehrotra, A. K. Measurement of the liquid−deposit interface temperature during solids deposition from wax−solvent mixtures under static cooling conditions. *Energy Fuels* **2008**, *22*, 1174.

(29) Bidmus, H.; Mehrotra, A. K. Measurement of the liquid−deposit interface temperature during solids deposition from wax−solvent mixtures under sheared cooling. *Energy Fuels* **2008**, *22*, 4039.

(30) Hsu, J. J. C.; Brubaker, J. P. Wax deposition and scale-up modeling for waxy live crudes under turbulent flow conditions. Society of Petroleum Engineers (SPE) International Meeting, Beijing, China, Nov 1995; SPE paper 29976.

(31) Hsu, J. J. C.; Santamaria, M. M.; Brubaker, J. P. Wax deposition of waxy live crudes under turbulent flow conditions. Society of Petroleum Engineers (SPE) 69th Annual Technical Conference and Exhibition, New Orleans, LA, Sept 1994; SPE paper 28480.

large thermal resistance of the deposit layer, the overall thermal resistance increases and the rate of heat transfer decreases. The deposit-layer thickness increases with time until becoming constant at steady state, when the rates of heat transfer from the flowing oil to the deposit layer, the pipe wall, and the surroundings become equal. That is, at thermal steady state, the thermal resistances offered by flowing liquid (convection), deposit layer (conduction), pipe wall (conduction), and surroundings (convection) reach constant values.[14−16]

For the double-pipe heat exchanger used co-currently in the flow-loop tests, the rate of heat transfer at steady state is equal to the rate of thermal energy lost by the wax−solvent mixture and the rate of thermal energy gained by the coolant, as follows:[14−16]

$$q = \dot{m}_h C_h (T_{hi} - T_{ho}) = \dot{m}_c C_c (T_{co} - T_{ci}) - q_{gain} = U_i A_i \frac{[(T_{hi} - T_{ci}) - (T_{ho} - T_{co})]}{\ln[(T_{hi} - T_{ci})/(T_{ho} - T_{co})]} \quad (1)$$

The combined thermal resistance is the sum of four thermal resistances in series, i.e.,

$$\frac{1}{U_i A_i} = \frac{1}{2\pi(r_i - x_d)Lh_h} + \frac{\ln(r_o/r_i)}{2\pi k_m L} + \frac{\ln(r_i/(r_i - x_d))}{2\pi k_d L} + \frac{1}{2\pi r_o L h_c} \quad (2)$$

Equation 2 can also be written as $R_{total} = R_h + R_d + R_m + R_c$, where $R_h \equiv [2\pi(r_i - x_d)Lh_h]^{-1}$, $R_d \equiv [(2\pi Lk_d)/\ln\{r_i/(r_i - x_d)\}]^{-1}$, $R_m \equiv [(2\pi Lk_m)/\ln\{r_o/r_i\}]^{-1}$, and $R_c \equiv [2\pi r_o L h_c]^{-1}$. By equating the rates of heat flow through the four thermal resistances in eq 2, we obtain

$$\frac{q}{A_i} = \frac{h_h(T_h - T_d)}{r_i/(r_i - x_d)} = \frac{k_d(T_d - T_{wi})}{r_i \ln(r_i/(r_i - x_d))} = \frac{k_m(T_{wi} - T_{wo})}{r_i \ln(r_o/r_i)} = \frac{h_c(T_{wo} - T_c)}{r_i/r_o} \quad (3)$$

where x_d is the average deposit-layer thickness, k_d is the average deposit thermal conductivity, and T_d is the liquid−deposit interface temperature. Note that eqs 2 and 3 involve two heat-transfer coefficients, h_h and h_c, which were estimated from the correlations developed previously.[16,26] For the constant coolant rate used in all experiments, h_c was estimated to be 2700 W m^{-2} K^{-1}. The heat-transfer coefficient for wax−solvent mixtures, h_h, varied with the flow rate (or Re) from approximately 1400 to 3600 W m^{-2} K^{-1}.[25] At $x_d/r_i > 0.02$, the deposit layer offered the dominant thermal resistance; hence, an uncertainty in h_h and h_c did not affect the heat-transfer calculations significantly.[25]

Using the experimental data or estimated values for q, A_i, T_h, T_c, h_h, h_c, r_i, r_o, x_d, and k_m, the four equalities in eq 3 were solved simultaneously to obtain T_{wi}, T_{wo}, T_d, and k_d. These unknowns include the two quantities of particular interest, namely, the liquid−deposit interface temperature, T_d, and the deposit average thermal conductivity, k_d.

Deposit Thermal Resistance. Bidmus and Mehrotra[14] proposed a dimensionless parameter, θ_d, which is the ratio of the deposit thermal resistance to the overall thermal resistance at steady state. Note that θ_d also represents the fractional thermal resistance offered by the deposit, and it is equal to the ratio of the temperature difference across the deposit to the overall thermal driving force. That is,

$$\theta_d \equiv \frac{R_d}{R_{total}} = \frac{T_d - T_{wi}}{T_h - T_c} \quad (4)$$

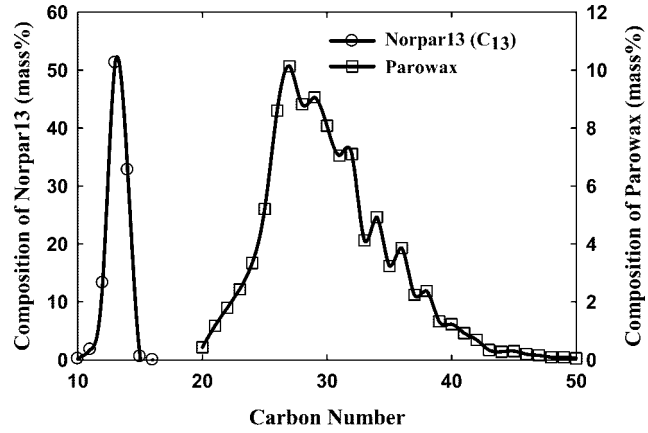

Figure 1. GC analysis of Norpar13 (solvent) and Parowax (wax).[15,16]

The calculations performed at typical experimental conditions used in this study showed that, with an increase in the deposit-layer thickness (x_d/r_i), θ_d increased sharply.[25] At $x_d/r_i > 0.02$, θ_d represented the controlling resistance, resulting in the largest temperature drop across the deposit. Similar results were also reported previously by Mehrotra and co-workers.[14−16]

Experimental Section

Materials. As mentioned previously, all deposition experiments were performed with prepared multicomponent wax−solvent mixtures. The wax (Parowax) used in this study was obtained from the Conros Corporation (Ontario, Canada). Parowax, with a melting point of 57−62 °C, consisted of *n*-alkanes in the range of C_{19}−C_{60}. The solvent used was Norpar13, which was obtained from Imperial Oil (Ontario, Canada), and it consisted of *n*-alkanes ranging from *n*-C_9 to *n*-C_{16}. Each batch of 10 and 15 mass % wax−solvent mixtures was prepared by mixing about 12 L of Norpar13 with the required mass of Parowax. Note that the 12 L batch size was large enough such that subsequent deposition experiments were not affected by a depletion of C_{20}^+ constituents in the wax−solvent mixture.[25] Each batch of wax−solvent mixtures was used for 10 deposition experiments. The mixture was held at 70 °C for 2−3 h to dissolve the wax and to erase any thermal history.

The WATs of 10 and 15 mass % Parowax−Norpar13 mixtures, measured using a visual method with cooling in steps of 1 °C, were 38 + 1 and 41 + 1 °C, respectively.[26] The viscosity, density, and specific heat capacity of 10 and 15 mass % Parowax−Norpar13 mixtures were estimated by interpolating the correlations reported by Fong and Mehrotra.[16]

GC Analyses. All GC analyses were performed on a HP 6890 series system, equipped with a fused-silica nonpolar column (10 m × 0.53 mm × 0.88 μm) and a hydrogen flame ionization detector (FID). The GC was calibrated using the American Society for Testing and Materials (ASTM) D2887 extended method, using a C_5−C_{59} hydrocarbon standard from Separation Systems (Gulf Breeze, FL). The GC analyses were normalized by neglecting the trace amounts of C_{42}−C_{59}.[25]

The carbon number distributions for Norpar13 and Parowax are shown in Figure 1. Norpar13 is a mixture of *n*-alkanes, ranging from C_9 to C_{16}, with C_{13} and C_{14} being the two main constituents. The average molar mass of Norpar13 is 186 kg $kmol^{-1}$, which corresponds to a carbon number of about 13. Parowax shows a broader distribution, with C_{26}−C_{29} being the main constituents. The average molar mass of Parowax is 414 kg $kmol^{-1}$, which corresponds to a carbon number of about 29.

Bench-Scale Flow-Loop Apparatus for Deposition Experiments. The details of the flow-loop apparatus, shown schematically in Figure 2, have been described elsewhere.[16,25,26] Briefly, it consisted of a co-current double-pipe heat exchanger, a wax−solvent mixture tank held in a temperature-regulated heating bath, a

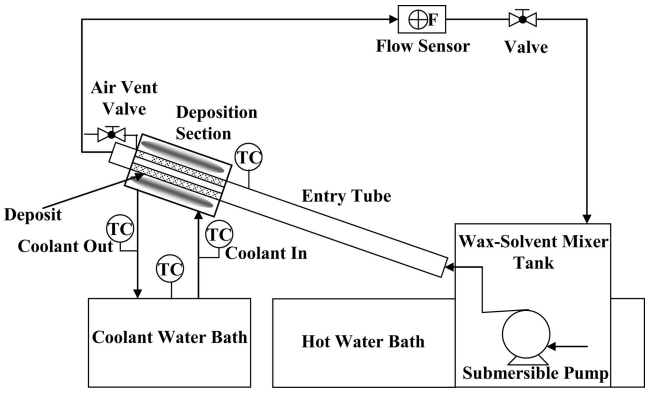

Figure 2. Schematic of the bench-scale flow-loop apparatus.

Table 1. Regression Constants in Eqs 6 and 7 for the Average Density of Deposit Samples from Deposition Experiments with 10 and 15 Mass % Parowax−Norpar13 Mixtures

constant	10 mass % wax	15 mass % wax
a_1 (kg m^{-3})	1689.6	957.84
a_2 (dimensionless)	6.5145	13.316
a_3 (dimensionless)	10.508	8.8226
a_4 (dimensionless)	26.841	530.31
a_5 (h)	4.5674	−12.642
a_6 (h)	1.9512	3.9904
α (kg m^{-3} °C^{-1})	−0.1888[a]	−0.1888

[a] Assumed to be the same as for the 15 mass % wax mixture.

Table 2. Design of Experiments for Solids Deposition from 10 and 15 Mass % Parowax−Norpar13 Mixtures

variable	number of levels	value(s) of variables tested
wax concentration (mass %)	2	10 and 15
Reynolds number of wax−solvent mixture (Re)	3 (with additional tests to verify repeatability)	9000 < Re < 27 000
wax−solvent mixture temperature, T_{hi} (°C)	1	WAT + 5 °C
coolant temperature, T_{ci} (°C)	1	WAT − 20 °C
deposition time (h)	6	0.5, 1, 2, 4, 12, and 24 h

submersible pump for recirculating the wax−solvent mixture, a temperature-regulated refrigerated bath with a centrifugal pump for circulating the coolant (water), a paddle-wheel-type flowmeter at the outlet end of the heat exchanger, a flow-regulating valve, and J-type calibrated thermocouples connected to a data logger. The coolant (water) was circulated through the annulus of the heat exchanger at a constant rate of 0.023 L s^{-1}. All of the exposed surfaces were adequately insulated, including the heat exchanger and a straight copper tube used for flow development before the heat exchanger inlet.

The deposition of solid occurred on the inner surface of a machined aluminum tube (with $r_i = 1.27$ cm, $r_o = 1.65$ cm, and $L = 10.16$ cm), while the coolant (water) flowed co-currently through the outer tube made of plexiglass (3.8 cm i.d. × 4.6 cm o.d. × 10.16 cm). Heat-transfer calculations showed that q_{gain} was less than 1% of the rate of heat transfer, q.[25,26] An air vent was provided at the outlet of the deposition section to allow for rapid draining of the wax−solvent mixture upon the termination of each experiment.

Procedure for Deposition Experiments. Before commencing a deposition experiment, the wax−solvent mixture was heated to 70 °C and held at this temperature for 2−3 h to dissolve the wax and to erase any thermal history. After the desired heating and cooling bath temperatures were attained, the wax−solvent pump and the data acquisition system were turned on. The deposition process was commenced by circulating the coolant (water) from the refrigerated bath through the annular side of the heat exchanger. The deposition experiment was terminated by stopping the submersible pump followed by quickly draining the wax−solvent mixture from the heat exchanger (by opening the air-vent valve); even a small delay in the draining process caused additional deposition.[25,26] The annulus of the wax deposition section was drained before isolating the deposition tube. The deposition tube was removed, and its outer surface was dried. The deposition tube was weighed to a precision of ±0.1 mg, and the deposit mass was obtained by difference. After its density was measured, a small sample of deposit was saved for the GC analysis and the rest was returned to the wax−solvent mixture, such that the composition of the wax−solvent mixture did not change appreciably for subsequent experiments. As mentioned previously, each batch of wax−solvent mixture was used for only 10 deposition experiments.

Average Deposit Density. An estimate of the density of the deposit layer (ρ_d) at its average temperature, $T_{d,avg} = (T_d + T_{wi})/2$, was required for calculating the average deposit-layer thickness (x_d) from the deposit mass (m_d), as follows:

$$x_d = r_i - \{r_i^2 - m_d/(\pi\rho_d L)\}^{0.5} \quad (5)$$

The average density of each deposit sample was measured at the laboratory temperature (23 °C) using a pycnometer. For the deposit samples from the experiments with 15 mass % mixture, the average deposit density was also measured at 33 °C. For estimating the deposit density at $T_{d,avg}$, the density data at 23 °C for deposit samples from the experiments with 10 and 15 mass % were regressed individually with the following equation:

$$\rho_{23\ °C} = a_1/[1 + \exp\{-(\log \mathrm{Re} - a_2)/a_3\}] + a_4/[1 + \exp\{-(t - a_5)/a_6\}] \quad (6)$$

Equation 6 was found to adequately correlate an increase in the deposit density with both Re and t in an asymptotic manner. The regression constants a_1−a_6 in eq 6 are listed in Table 1. The measured densities at 23 and 33 °C of the deposit samples from experiments with the 15 mass % mixture were fitted to the following linear equation:

$$\rho_{d,avg} = \rho_{23\ °C} + \alpha(T_{d,avg} - 23.0) \quad (7)$$

where α is a constant, also listed in Table 1. The average deviation between the measured and calculated deposit densities was 0.35%. Because the density of deposit samples from the 10 mass % mixture was measured only at 23 °C, α obtained from eq 7 was also used for estimating $\rho_{d,avg}$ for the experiments with the 10 mass % mixture.

Design of Experiments. On the basis of the previous deposition studies in turbulent and laminar flow regimes,[14−16] the Reynolds number (or shear rate) and deposition time were selected as the two primary variables for this study. The deposition experiments were performed according a factorial design of experiments summarized in Table 2. For all deposition experiments, the inlet wax−solvent mixture temperature (T_{hi}) and the inlet coolant temperature (T_{ci}) were held at WAT + 5 °C and WAT − 20 °C, respectively. Three wax−solvent mixture flow rates, ranging from 40 to 100% of the maximum pump capacity of 1.2 L s^{-1}, were used. The corresponding Reynolds numbers were between 9000 and 27 000. A coolant flow rate of 0.023 L s^{-1} was used in all experiments, which yielded a high heat-transfer coefficient (h_c) or a small thermal resistance (R_c) while allowing a reasonably large temperature difference ($T_{co} - T_{ci}$).[25] To investigate the deposit aging phenomenon, the experiments were performed over deposition times from 30 min to 24 h. Additional deposition experiments were performed to verify their repeatability, which yielded a measurement error of less than 4.5% for the deposit mass.[25]

Results and Discussion

Results from all of the deposition experiments are presented and discussed in the following three subsections. Detailed results for all of the experiments have been reported in the Master's thesis by Tiwary.[25] First, the deposition results are presented

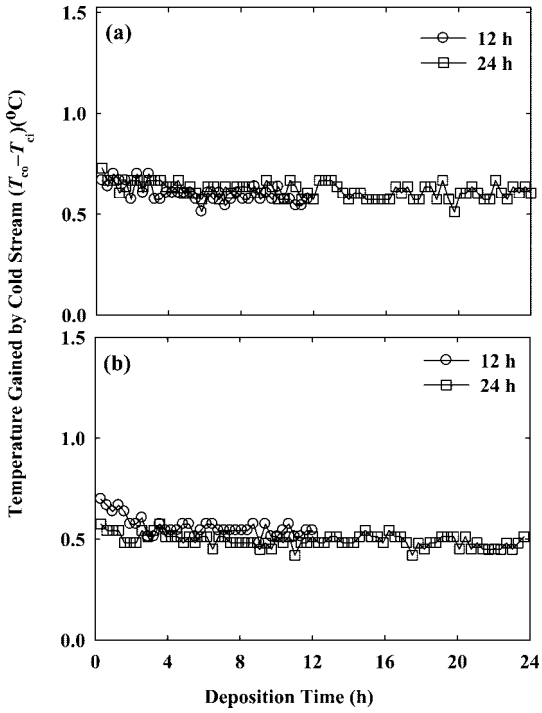

Figure 3. Approach to thermal steady-state in deposition experiments: (a) 10 mass % wax−solvent mixture and (b) 15 mass % wax−solvent mixture.

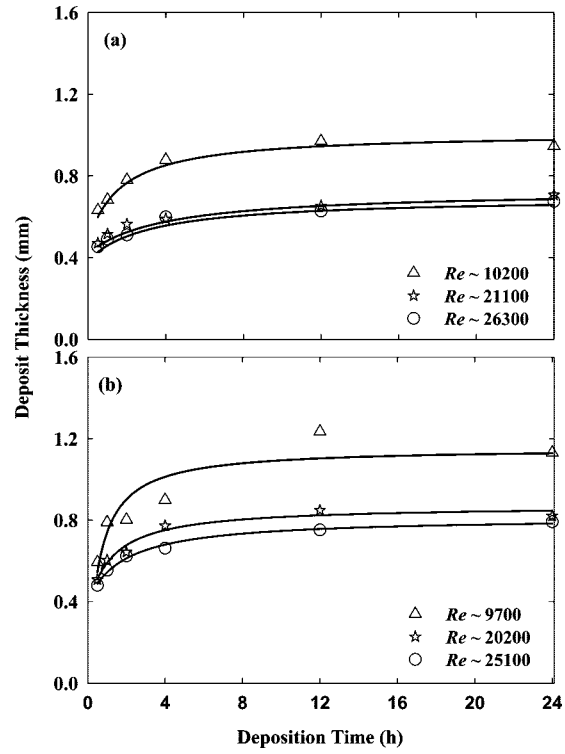

Figure 4. Variation in deposit thickness, x_d, with deposition time, t, at different Reynolds numbers, Re: (a) 10 mass % wax−solvent mixture and (b) 15 mass % wax−solvent mixture.

from experiments at different Reynolds numbers (Re) and deposition times (t) for 10 and 15 mass % wax−solvent mixtures. As shown in Table 2, these experiments were performed over six deposition times (0.5, 1, 2, 4, 12, and 24 h) and three Reynolds numbers (9000 < Re < 27 000) for 10 and 15 mass % wax−solvent mixtures. Next, the results from GC analyses on deposit samples are presented to highlight the changes in their carbon number distributions caused by variations in the composition of wax−solvent mixtures, Re, and t. Finally, a mathematical model is presented for the deformation angle (β), which is a parameter included in the cubical-cage representation by Mehrotra and Bhat,[27] to account for the effects of Re (or shear rate) and t on the deposit composition.

Deposition Results. All of the deposition experiments performed in this study indicated that a thermal steady state was reached within 30 min, which was confirmed by a constant value of the gain in coolant temperature in eq 1, ($T_{co} - T_{ci}$). Plotted in Figure 3 are the measured ($T_{co} - T_{ci}$) for the experiments with 10 and 15 mass % wax−solvent mixtures at Re = 10 200 and 9700, respectively, conducted over 12 and 24 h. In all deposition experiments, ($T_{co} - T_{ci}$) was high initially but decreased rapidly to less than 1 °C within about 2−3 min, and the thermal steady state was reached in about 20−30 min and was not altered appreciably thereafter. For the same Reynolds number, each plot in Figure 3 shows the same constant value of ($T_{co} - T_{ci}$), which indicates that the rate of heat transfer did not change from 20−30 min to 24 h. These results confirm the observation made in previous deposition studies,[14−16] which also showed the deposition process to be relatively fast. However, this observation is applicable for the 10 cm deposition tube length; the time to reach steady state for longer pipe lengths would be higher, as shown by Bhat and Mehrotra.[22−24]

Previous studies[10,20,21,30,31] have reported sloughing or shearing off of the deposits because of the high rate of shear at the wall caused by high flow rates under turbulent flow conditions. Sloughing is believed to occur when the shear rate overcomes the cohesive and adhesive forces of the paraffin wax molecules to the surface.[20] However, an analysis of the recorded temperatures did not show any abrupt change to indicate sloughing (and regrowth) of the deposit in any of the deposition tests performed in this study. A previous study[16] using a similar deposition apparatus also did not report any sloughing in the tests lasting over shorter deposition times of up to 8 h.

Figure 4 shows variations in the average deposit-layer thickness with the deposition time for both 10 and 15 mass % wax−solvent mixtures at three Reynolds numbers. It was observed that, at the same Re, the "hardness" of deposit samples increased with an increased deposition time. The deposit thickness increased asymptotically with t, but it decreased with an increase in Re. The increase in the deposit thickness with deposition time is more pronounced at the lowest Re of about 10 000. It was also noted that the deposit thickness did not change beyond t = 12 h; the deposit thicknesses at 12 and 24 h were noted to be within about ±5%. Furthermore, a comparison of the results in Figures 3 and 4 indicates that the increase in deposit thickness from t = 30 min to 12 h did not alter the rate of heat transfer.

Liquid−Deposit Interface Temperature (T_d) and Deposit Thermal Conductivity (k_d). All of the deposition data were analyzed using eqs 1 and 3 by solving the four equalities in eq 3 for T_{wi}, T_{wo}, T_d, and k_d. The average values of T_d and k_d for the deposition experiments with both 10 and 15 mass % wax−solvent mixtures are listed in Table 3. As shown in Figure 5, all of the estimated values of T_d from deposition experiments, over 30 min < t < 24 h, are close to the experimentally measured WAT for both mixtures. The estimated values of T_d, for both 10 and 15 mass % wax−solvent mixtures, did not show any statistically significant variation with t. Thus, the T_d results do not support the increasing interface temperature assumption in the molecular diffusion (or concentration gradient) modeling approach for wax deposition. That is, $T_d \approx$ WAT, which has been observed in other deposition studies[14−16] as well as in two

Table 3. Average Values of the Liquid−Deposit Interface Temperature (T_d) and Deposit Thermal Conductivity (k_d) Estimated from Heat-Transfer Analysis of Data at Different Deposition Times

	liquid−deposit interface temperature, WAT, or T_d (°C)		average deposit thermal conductivity, k_d (W m^{-1} K^{-1})	
Parowax−Norpar13 mixture	measured WAT[16]	estimated T_d	estimated from eq 3	estimated from eq 8
10 mass % wax	38−39	40.9 ± 0.9	0.21 ± 0.10	0.35 ± 0.11
15 mass % wax	41−42	41.8 ± 1.2	0.35 ± 0.11	0.35 ± 0.11

recent studies involving batch cooling of different wax−solvent mixtures under static and sheared conditions.[28,29]

The average deposit thermal conductivities for 10 and 15 mass % wax−solvent mixtures in Table 3 are different at 0.21 and 0.35 W m^{-1} K^{-1}, respectively. The calculations indicated that, in the first equality in eq 3, T_d was not sensitive to variations in x_d, when $x_d/r_i \ll 1$. However, the second equality in eq 3 (i.e., for the deposit layer) involves k_d along with both T_d and x_d, which made the calculated k_d quite sensitive to x_d. That is, an experimental uncertainty in x_d caused a relatively large variation in the estimated k_d. In an attempt to minimize the scatter in the estimated k_d, the calculations were repeated by setting T_d = WAT in eq 3, which simplified it to involve only three equalities, as follows:

$$\frac{h_h(T_h - \mathrm{WAT})}{r_i/(r_i - x_d)} = \frac{k_d(\mathrm{WAT} - T_{wi})}{r_i \ln(r_i/(r_i - x_d))} = \frac{k_m(T_{wi} - T_{wo})}{r_i \ln(r_o/r_i)} = \frac{h_c(T_{wo} - T_c)}{r_i/r_o} \quad (8)$$

Using eq 8, the average deposit thermal conductivities for both 10 and 15 mass % wax−solvent mixtures were found to be about the same, i.e., $k_d = 0.35 \pm 0.11$ W m^{-1} K^{-1}.[25] Note that this predicted average value of k_d is within the range of the thermal conductivities of Norpar13 (0.14 W m^{-1} K^{-1})[15,16] and solid *n*-eicosane (0.42 W m^{-1} K^{-1}).[32] The standard deviation of 0.11 W m^{-1} K^{-1} in the estimated average k_d for both wax−solvent mixtures is attributed to the variations in Reynolds number and deposition time as well as experimental errors.

In Figure 6, the estimated k_d is seen to increase with Re at all deposition times. In both plots of Figure 6, k_d increases asymptotically up to $t \approx 12$ h and then becomes constant. This trend is similar qualitatively to that for the variation of x_d in Figure 4.

Figure 7 describes the relationship between the deposit thermal conductivity, k_d, and the average deposit density, ρ_d,

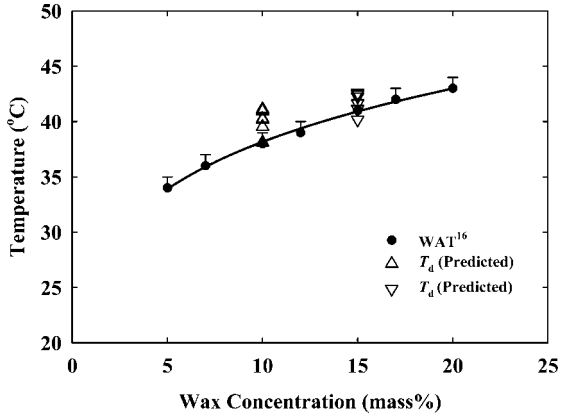

Figure 5. Comparison of the calculated liquid−deposit interface temperature (T_d) with WAT measurements[16] for Parowax−Norpar13 mixtures.

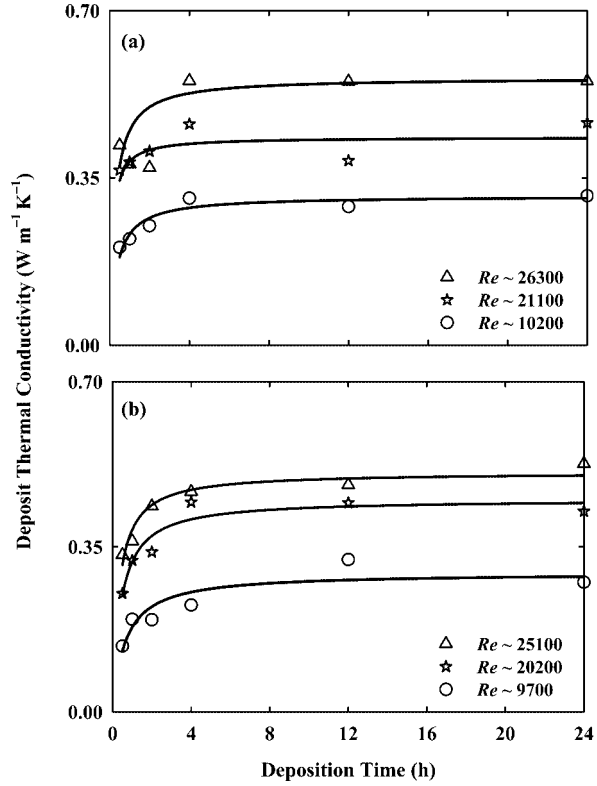

Figure 6. Variation in average deposit thermal conductivity, k_d, with deposition time at different Reynolds numbers: (a) 10 mass % wax−solvent mixture and (b) 15 mass % wax−solvent mixture.

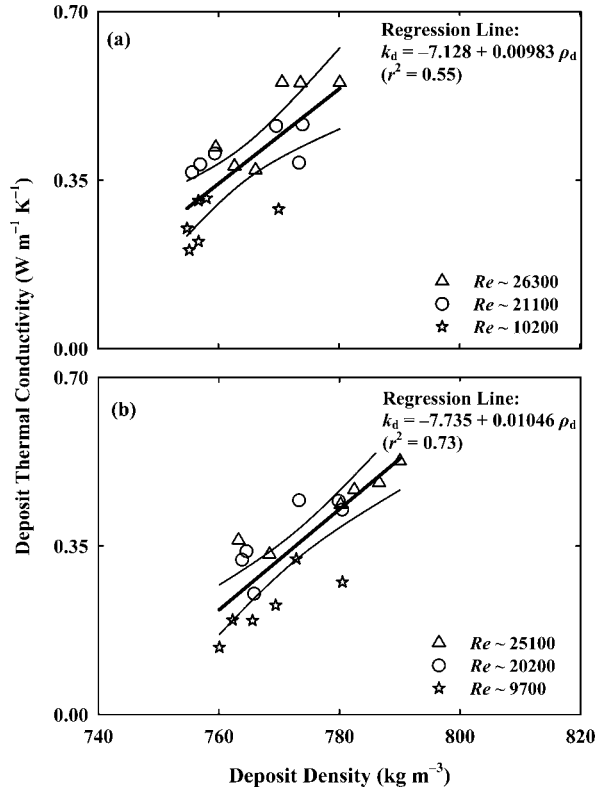

Figure 7. Dependence of average deposit thermal conductivity, k_d, on deposit density, ρ_d: (a) 10 mass % wax−solvent mixture and (b) 15 mass % wax−solvent mixture.

for both 10 and 15 mass % wax−solvent mixtures. Despite the scatter in Figure 7, k_d is seen to increase with an increase in ρ_d,

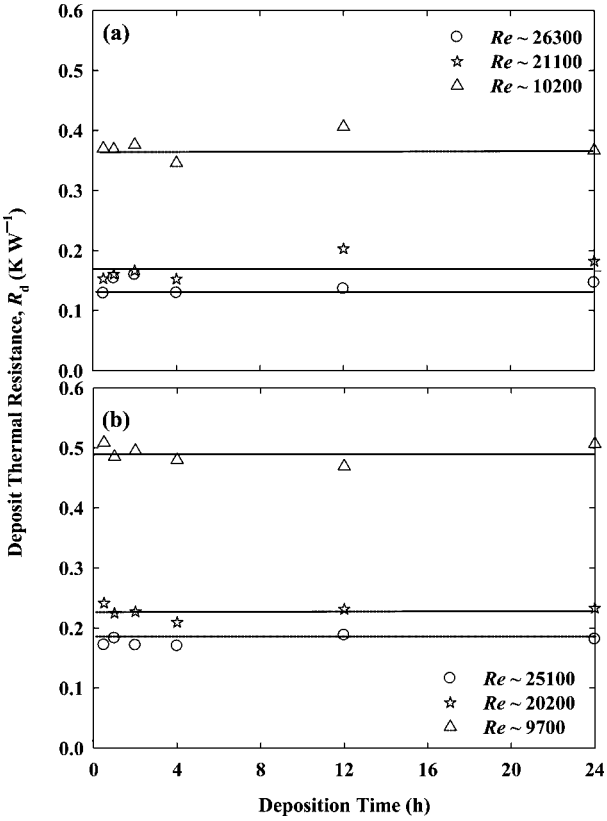

Figure 8. Variation in deposit thermal resistance, R_d, with the deposition time at different Reynolds numbers: (a) 10 mass % wax−solvent mixture and (b) 15 mass % wax−solvent mixture.

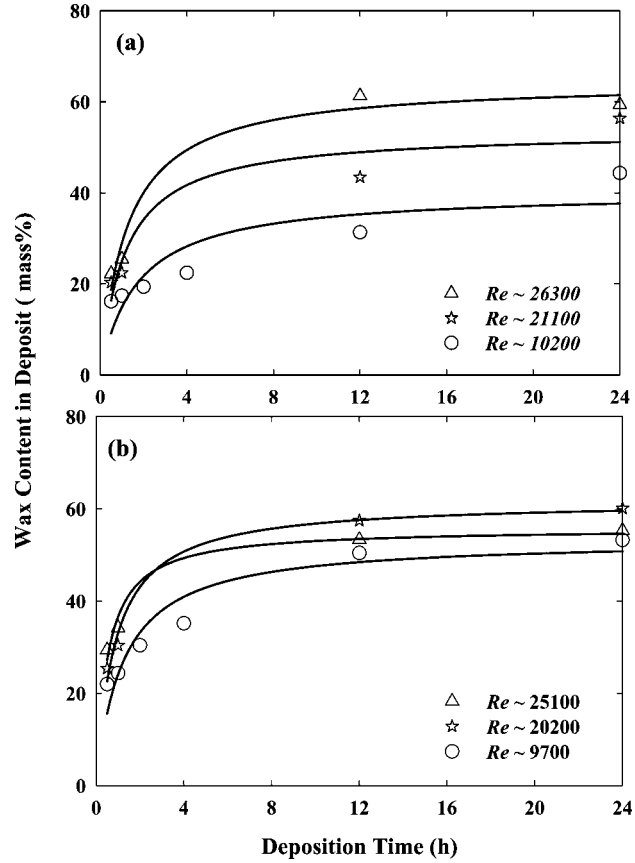

Figure 9. Variation in the deposit wax content with deposition time at different Reynolds numbers: (a) 10 mass % wax−solvent mixture and (b) 15 mass % wax−solvent mixture.

as indicated by the linear regression lines in both plots, which can be attributed to an increase in the deposit solid-phase content.

Deposit Thermal Resistance (R_d). All of the results for the calculated deposit thermal resistance, R_d, are plotted against the deposition time (t) in Figure 8. The results show that R_d decreases with an increase in Re. It also shows that, for each wax−solvent mixture at a constant Re, R_d remains constant with t. Because all other thermal resistances (i.e., R_h, R_m, and R_c) do not vary with t, the results in Figure 8 suggest that the fractional thermal resistance of the deposit, θ_d, also remained constant over $0.5 < t < 24$ h.[25] This is an important result, which indicates that R_d or θ_d does not change with t, even though the deposit-layer thickness (x_d in Figure 4), the deposit density ($\rho_{23\ °C}$ according to eq 6) and the deposit thermal conductivity (k_d in Figure 6) were observed to increase asymptotically with t.

One possible explanation for R_d or θ_d to not change with t, as seen in Figure 8, could be that the liquid-phase fraction in the deposit decreased with t, causing a corresponding increase in the solid-phase fraction. A decrease in the liquid-phase fraction (and a corresponding increase in the solid-phase fraction) would cause both the density and thermal conductivity of the deposit to increase with t, as noted above. An increase in k_d would necessitate an increase in x_d or m_d for the thermal resistance of the deposit layer to satisfy the heat-flux equalities in eq 3 or 8. The changes in k_d, ρ_d, and x_d would continue with time as long as the liquid- and solid-phase fractions in the deposit continue to change. These observations present an interesting and complex effect of Re (or shear rate) and t on the deposit thickness, density, thermal conductivity, composition, and solid−liquid phase ratio.

Wax Content of Deposit. As mentioned previously, the deposit formed from "waxy" mixtures consists of solid and liquid phases. An analysis of the deposit layer at *in situ* conditions would be difficult because the liquid- and solid-phase fractions are sensitive to changes in the thermal and hydrodynamic conditions. Likewise, it may not be possible to separate and analyze the two phases while maintaining the deposit at the experimental conditions. The wax content of the deposit was, therefore, estimated from GC analysis, which provided its bulk composition in terms of the mass fractions of n-alkanes ranging from C_8 to C_{40}. Because all carbon numbers less than 19 belonged to the solvent (Norpar13) and higher than 20 belonged to the wax (Parowax), the sum of mass fractions for n-alkanes heavier than C_{20} was taken to be the wax content of the deposit. Thus, the deposit wax content was defined as $\sum_{j=21}^{41} (w_d)_j$, where $(w_d)_j$ is the mass fraction of the jth n-alkane in the deposit. It is noted that the deposit wax content does not correspond directly to the solid-phase mass fraction in the deposit because the bulk analysis of the deposit would include C_{20}^+ constituents in the solid phase as well as in the liquid phase (trapped within the deposit).

The results for the wax content of deposit samples are plotted in Figure 9, which shows the deposit−wax content to increase asymptotically with the deposition time, with no appreciable change beyond 12 h. The trends in Figure 9 are generally similar to those in Figures 4 and 6 for the variation of x_d and k_d, respectively. In Figure 9a, the deposit wax content is seen to increase with an increase in the Reynolds number for the 10 mass % wax−solvent mixture. In Figure 9b, the effect of the Reynolds number on the deposit wax content for the 15 mass

(32) Stryker, P. C.; Sparrow, E. M. Application of a spherical thermal conductivity cell to solid n-eicosane paraffin. *Int. J. Heat Mass Transfer* **1990**, *33*, 1781.

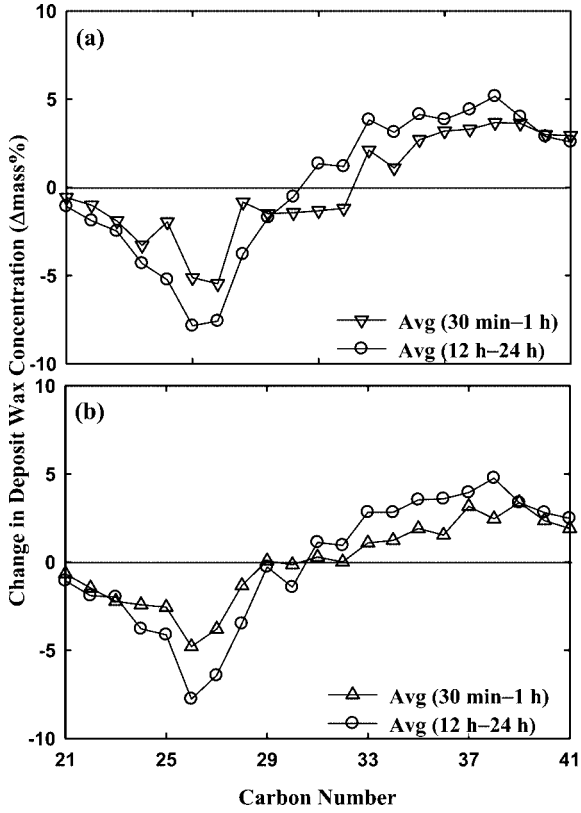

Figure 10. Changes in deposit wax composition at small and large deposition times (for Re ~ 26 300): (a) 10 mass % wax−solvent mixture and (b) 15 mass % wax−solvent mixture.

% wax−solvent mixture is not as pronounced, especially for Re > 20 200 and t > 2 h.

Deposit Compositional Changes. To highlight the changes in the carbon number distribution of deposit samples, the mass fractions of C_{21}−C_{41} in the deposit were compared to those in the original wax−solvent mixture. The normalized (solvent-free) mass fractions of *n*-alkane with the *i*th carbon number in the deposit, $(W_d)_i$, and in the wax−solvent mixture, $(W_h)_i$, were calculated as follows:[16]

$$(W_d)_i = (w_d)_i / \sum_{j=21}^{41} (w_d)_j \text{ and } (W_h)_i = (w_h)_i / \sum_{j=21}^{41} (w_h)_j \qquad (9)$$

The difference between the above two normalized (solvent-free) mass fractions, $[(W_d)_i - (W_h)_i]$, represented the change in the composition of *n*-alkane with the *i*th carbon number.

Figures 10 presents the variation in $[(W_d)_i - (W_h)_i]$ for *n*-alkanes from C_{21} to C_{41} for 10 and 15 mass % wax−solvent mixtures at the highest Reynolds number of about 26 300. Note that, in each plot of Figure 10, symbols represent the average results for the two shortest deposition times (0.5 and 1 h) and the two longest deposition times (12 and 24 h). The trends in Plots a and b of Figure 10 for 10 and 15 mass % wax−solvent mixtures are very similar. For the short deposition time of 0.5−1 h, the minimum and the maximum differences corresponding to C_{26} and C_{38} are −6 and +4 Δmass %, respectively. However, for the long deposition time of 12−24 h, the differences corresponding to C_{26} and C_{38} are much larger at −8 and +6 Δmass %, respectively. These results indicate that, even at a short deposition time of 0.5−1 h, the deposit becomes enriched in *n*-alkanes heavier than C_{29}−C_{30}, while it becomes depleted in those lighter than C_{29}−C_{30}, and the extent of such enrichment and depletion tendency increases with the deposition time. Similar trends in the deposit composition were also observed at lower Reynolds numbers.[25]

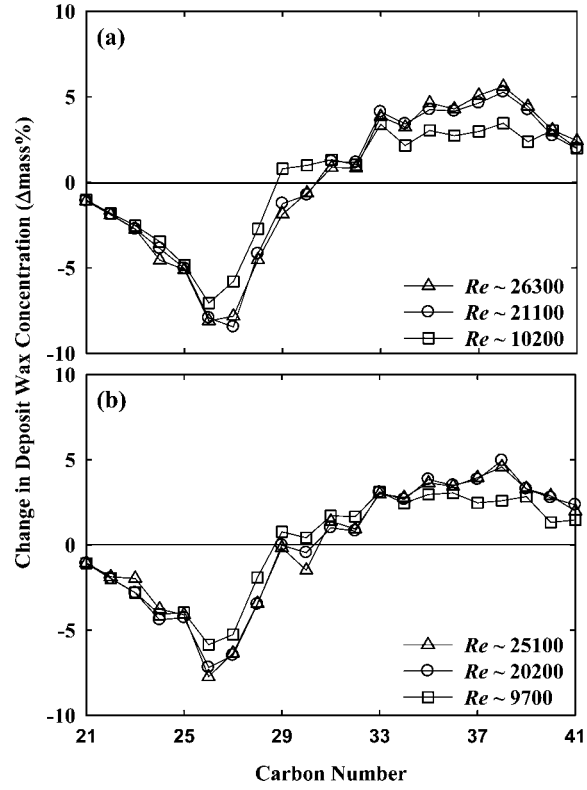

Figure 11. Changes in deposit wax composition for different Reynolds numbers, Re (at t = 24 h): (a) 10 mass % wax−solvent mixture and (b) 15 mass % wax−solvent mixture.

Figure 11 shows similar changes in the deposit composition for different Reynolds numbers, at the longest deposition time of 24 h, for 10 and 15 mass % wax−solvent mixtures. It is seen that an increase in the Reynolds number also causes an increased enrichment of *n*-alkanes heavier than C_{29}−C_{30} and an increased depletion of *n*-alkanes lighter than C_{29}−C_{30}; however, the effect of the Reynolds number on the enrichment and depletion tendency is not as pronounced as that of the deposition time in Figure 10. Similar changes in the deposit composition with changes in Reynolds number were also observed for shorter deposition times.[25]

The time-dependent change in the deposit composition is commonly referred to as the "deposit aging" phenomenon.[11,13,17] The results in Figures 10 and 11, as well as those in Figure 9, show that both Reynolds number and deposition time cause changes in the wax content and carbon number distribution of the deposit. However, the effect of the wax concentration in the wax−solvent mixture is relatively not as significant. Overall, these results show that the deposit becomes enriched in *n*-alkanes heavier than C_{29}−C_{30} and depleted in *n*-alkanes lighter than C_{29}−C_{30}, and this enrichment and depletion tendency increases with the deposition time and Reynolds number. That is, the carbon number of C_{29}−C_{30} is a "crossover" carbon number for the enrichment and depletion tendency, which is close to the mean carbon number of C_{29} for Parowax. Previous studies[11,17,24,27] have described this crossover carbon number to be dependent upon thermodynamic equilibrium considerations and the deposit temperature.

Modeling the Effects of Shear Stress and Deposition Time on Deposit Composition. The changes in deposit composition with time, as shown in Figures 9 and 10 that have been referred to as the "deposit aging", have been explained in terms of counter-diffusion of lighter and heavier constituents within the deposit.[2,11,13,17] Mehrotra and Bhat[27] proposed a

different approach to explain the changes in deposit composition, which involves modeling the effect of shear stress on the deposit caused by the flowing wax−solvent mixture. This model is based on one-dimensional deformation of a cubical cage, which causes the release of a fraction of liquid from the deposit, leading to wax enrichment and a shift in the carbon number distribution in the deposit. It was emphasized that the cubical-cage representation is not intended to match the configuration in which the solid and liquid phase might actually coexist in the gel-like deposit or the crystalline or structured nature of the solid phase within the deposit.[27] In the shear-induced model, the effect of shear stress is expressed in terms of a deformation angle, which for the laminar flow deposition data[14,15] was shown to depend upon the fractional deposit thermal resistance, deposit mass or thickness, and Reynolds number.[27] Recently, the cubical-cage deformation model was combined with the moving boundary problem approach for solids deposition in a pipeline.[24]

A brief description of the cubical-cage deformation model is given below, and further details are available elsewhere.[24,27] The deposit formed under static conditions (i.e., without any shear stress) is assumed to be a lattice-like structure with a unit cell that resembles a cubical cage of side a and volume V ($=a^3$). Each edge of the cubical cage is assumed to be rectangular in cross-section, $\xi \times \xi$, such that the ratio of the edge thickness to the side of the cubical cage is $Z = \xi/a$. The solid- and liquid-phase volume fractions in the cubical cage are

$$V_S = (12Z^2 - 16Z^3);\ V_L = (1 - 12Z^2 + 16Z^3) \qquad (10)$$

The application of a one-dimensional shear rate in the flow direction was assumed to tilt the cubical cage by an angle β.[27] The solid- and liquid-phase volume fractions in the tilted cage are

$$V_{S\beta} = (V_S V)/V_\beta = (12Z^2 - 16Z^3)/(\cos\beta);\ V_{L\beta} = [1 - (12Z^2 - 16Z^3)/(\cos\beta)] \qquad (11)$$

The actual volume of the liquid released from the cubical cage, because of its tilting by a deformation angle of β, is equal to the overall volume change, i.e.,

$$V - V_\beta \equiv (V_L V - V_{L\beta} V_\beta) = (1 - \cos\beta)a^3 \qquad (12)$$

In eq 11, $V_{S\beta} = 1$ or $V_{L\beta} = 0$ would occur at $\beta_{max} = \cos^{-1}(12Z^2 - 16Z^3)$, which corresponds to the complete release of all of the liquid from the tilted cage; that is, $\beta \le \cos^{-1}(12Z^2 - 16Z^3)$. The above relationships for the cubical-cage representation involve only two parameters, Z and β. Parameter Z in eq 10 corresponds to the initial cubical cage, i.e., without any shear stress; hence, it depends upon the volume fractions of liquid and solid phases in the deposit, which as mentioned before may not be measured directly. Instead, the volume fractions are estimated from liquid−solid phase equilibrium calculations at the deposition temperature.[27]

To simplify the thermodynamic calculations, the Parowax−Norpar13 mixture was represented by a pseudo-binary mixture, comprising C_{13} and C_{29}, which was assumed to form an ideal eutectic mixture (i.e., without any heat of mixing and volume change).[22] The liquidus temperature was calculated from the ideal eutectic relationship for binary mixtures.[4,22,23,27] The solid- and liquid-phase mass fractions in the cubical cage were obtained by applying the lever rule at the average deposit temperature.[25,27] For the tilted cage, the solid-phase mass fraction was obtained from the GC analysis of the deposit. For calculating the solid-phase volume fraction, the average densities of Parowax and Norpar13 were used. The above procedure was repeated for each deposit sample to obtain the corresponding

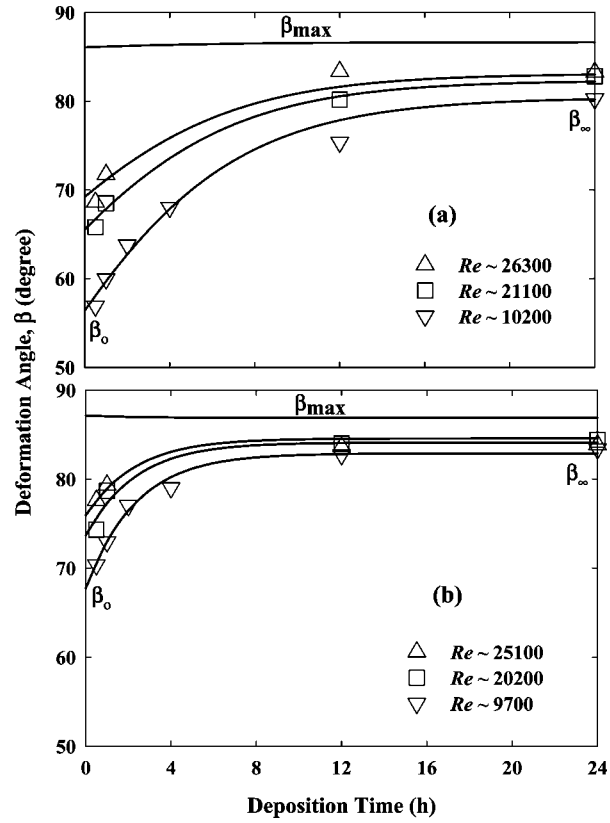

Figure 12. Dependence of the deformation angle, β, on the Reynolds number, Re, and the deposition time, t (the curves represent predictions from eq 15): (a) 10 mass % wax−solvent mixture and (b) 15 mass % wax−solvent mixture.

average deformation angle, β, and the results are plotted in Figure 12 for both 10 and 15 mass % wax−solvent mixtures.

A Viscoplastic Model for Deposit. Figure 12 shows the calculated values of the deformation angle, β, to increase asymptotically with both the deposition time (t) and the Reynolds number (Re). On the basis of this observation, it was postulated that the deposit layer, during its formation and growth, undergoes an irreversible time-dependent deformation caused by the shear stress. The term viscoplasticity has been used commonly to describe the time-dependent plastic deformation in polymers and mixtures, which when exposed to a shear stress display both instantaneous (plastic) and time-dependent (viscous) changes.

In developing a viscoplastic model to describe the changes in deposit composition, the deformation angle, β, was assumed to depend upon the Reynolds number, Re (assumed to cause initial changes), and the deposition time, t (assumed to cause time-dependent changes). The effect of t on β was assumed to be described by the following relationship:

$$\beta = \beta_o + (\beta_\infty - \beta_o)f(t) \qquad (13)$$

In eq 13, $f(t) = 0$ at $t \approx 0$; hence, β at $t = 0$ is denoted by β_o. Also, $f(t) = 1$ as $t \to \infty$; hence, β at $t \to \infty$ is denoted by β_∞. Furthermore, it was assumed that β approaches asymptotically its upper limit, β_{max}, at a very high Re, which can be expressed as

$$\beta \to \beta_{max}[\equiv \cos^{-1}\{12Z^2 - 16Z^3\}] \text{ at Re} \to \infty \qquad (14)$$

To satisfy the constraints in eqs 13 and 14 for modeling the data shown in Figure 12, the two upper limits for Re and t were assumed as follows: $\beta \to \beta_\infty$ at $t = 24$ h and $\beta \to \beta_{max}$ at Re $= 3 \times 10^6$ (which is greater than 100 times the highest Re used

Table 4. Regression Constants in Eq 15 for 10 and 15 Mass % Parowax−Norpar13 Mixtures

constant	10 mass % wax	15 mass % wax
b_1 (deg)	0.0	−166.65
b_2 (deg)	79.394	248.80
b_3 (h)	−2.8163	−5.6580
b_4 (h)	4.5554	2.2148
b_5 (deg)	85.023	257.13
b_6 (dimensionless)	4.4113	4.3917
b_7 (dimensionless)	0.22010	0.23757
b_8 (deg)	−77.767	−252.39

in the deposition experiments). Of the several functional forms evaluated for correlating β with Re and t, the following sigmoid (or logistic cumulative) equation was found to provide a good fit of the data:

$$\beta = b_1 + \frac{b_2}{1+\exp\left[-\frac{t-b_3}{b_4}\right]} + \frac{b_5}{1+\exp\left[-\frac{\log \mathrm{Re}-b_6}{b_7}\right]} + \frac{b_8}{1+\exp\left[-\frac{t-b_3}{b_4}\right]}\frac{1}{1+\exp\left[-\frac{\log \mathrm{Re}-b_6}{b_7}\right]} \quad (15)$$

In eq 15, b_1-b_8 are empirical constants, listed in Table 4, which were estimated by nonlinear regressions individually for 10 and 15 mass % wax−solvent mixtures. The average absolute deviations were 1.2 and 0.7% for the 10 and 15 mass % wax−solvent mixtures, respectively. For both sets of β values, the degrees-of-freedom adjusted r^2 was greater than 0.98.

Figure 12 shows a comparison of the β values corresponding to the GC analyses of deposit samples (shown by symbols) and those predicted from eq 15 (shown by curves). As indicated in plots a and b of Figure 12, the β values at $t = 0$ and 24 h represent β_o and β_∞, respectively. In both plots of Figure 12, β increases asymptotically, with an increase in t, from β_o to β_∞. Also, β increases asymptotically, with an increase in Re, to β_{max}. Thus, eq 15 is seen to provide a satisfactory representation of the effects of both t and Re on the deposit composition.

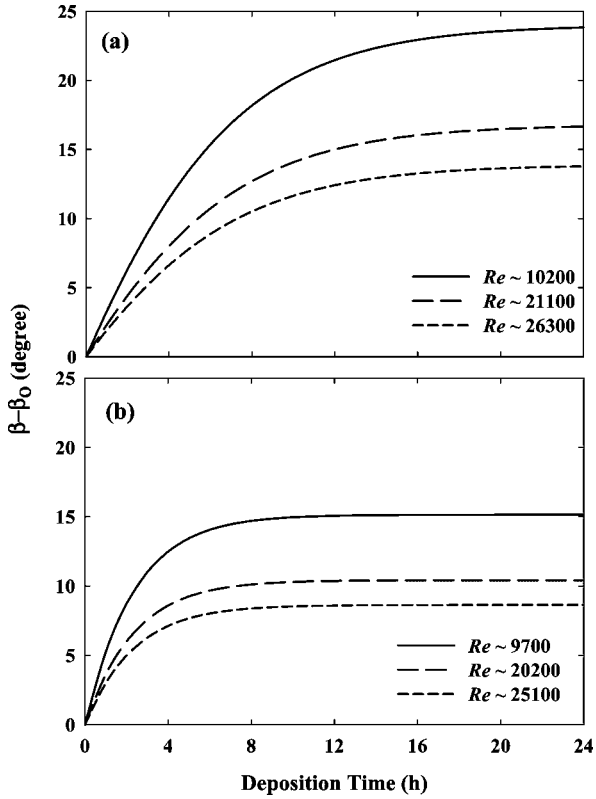

Figure 13. Predictions for the time-dependent viscous component of the deformation angle, ($\beta - \beta_o$), from eq 15: (a) 10 mass % wax−solvent mixture and (b) 15 mass % wax−solvent mixture.

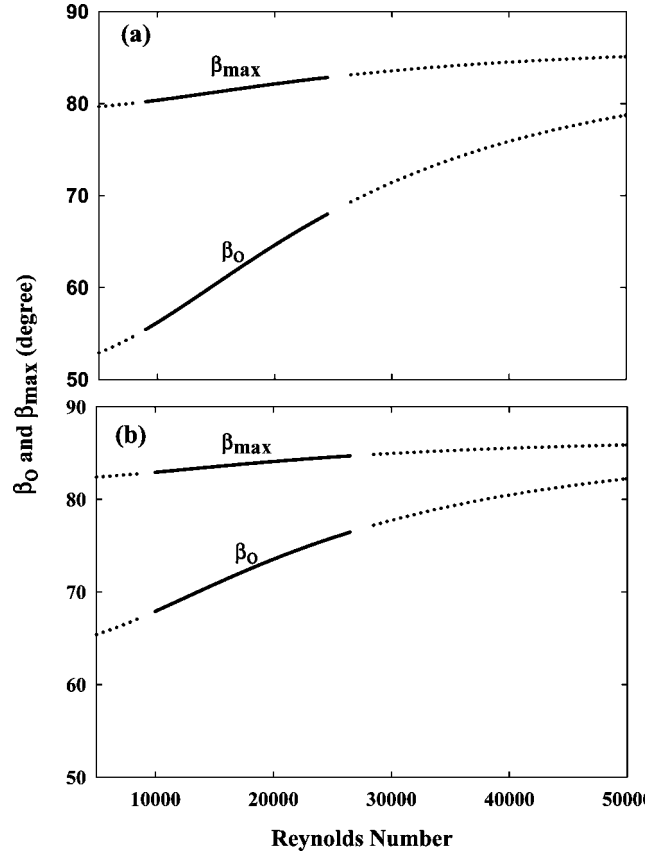

Figure 14. Predictions for the initial and maximum deformation angles, β_o and β_{max}, from eq 15: (a) 10 mass % wax−solvent mixture and (b) 15 mass % wax−solvent mixture.

In Figure 13, the predicted time-dependent (or the viscous) component of the deformation angle, ($\beta - \beta_o$), is plotted against the deposition time. The viscous component of the deformation angle increases asymptotically with t; however, it decreases with an increase in Re. The effects of the Reynolds number on β_o (at $t = 0$) and β_{max} (at Re $\rightarrow \infty$) are shown in Figure 14. Note that β_o represents the initial deformation of the deposit, while β_{max} represents the maximum possible deformation at a very high Reynolds number, when all of the liquid-phase would be squeezed out to make the deposit completely solid. In Figure 14, the solid curves are plotted for the range of Reynolds number (i.e., 9000 < Re < 27 000) corresponding to the data, while the dotted curves are extrapolated values, i.e., for Re < 9000 and Re > 27 000. The two plots in Figure 14 show both β_o and β_{max} to increase with Re and the wax concentration in Parowax−Norpar13 mixtures.

Overall, the viscoplastic characteristic of the deposit is described adequately by eq 15, as confirmed by the predictions in Figures 12−14. Equation 15 accounts for the combined effect of the deposition time and shear rate (expressed as Re). Because eq 15 (together with the empirical constants listed in Table 4) has been developed using the ideal eutectic thermodynamic model for the liquid−solid phase equilibrium together with the Parowax−Norpar13 mixture represented as a pseudo-binary mixture of C_{13} and C_{29} to predict the composition of deposit samples, its use for other wax−solvent mixtures or "waxy" crude oils should be performed with caution.

It is pointed out that the deformation angle, β, is related directly to the deposit composition (i.e., the solid and liquid volume fractions in the deposit, as given by eq 11) and only indirectly to the deposit thickness. As explained previously, the deposit thickness is dictated by its thermal resistance, R_d, which as shown in Figure 8 did not change with time in all of the experiments because of changes in the deposit density (expressed by eqs 6 and 7) and thermal conductivity (shown in Figure 6), both of which varied with time because of changes in β (i.e., the solid and liquid volume fractions in the deposit), as shown in Figure 12.

Finally, it is emphasized that the viscoplastic deformation approach, developed in this study, is an alternate explanation for the "deposit aging" phenomenon, which in previous studies[11,17] has been interpreted mainly as a time-dependent counter-diffusion process. In future studies, a mechanistic model could be developed for the shear-induced deformation approach to explain deposit aging.

Conclusions

This study investigated the effects of shear rate (or Reynolds number) and deposition time on solids deposition from prepared multicomponent "waxy" mixtures. The deposition experiments were performed using a bench-scale flow-loop apparatus, incorporating a double-pipe heat exchanger, with two wax concentrations (10 and 15 mass %), at three Reynolds numbers in the turbulent flow regime ($9000 < Re < 27\,000$) and for six deposition times (0.5, 1, 2, 4, 12, and 24 h). The deposition process was found to be quite fast, requiring less than 30 min to reach a thermal steady state. Sloughing or shearing off (and regrowth) of the deposit was not observed in any of the deposition tests. The deposition data were analyzed using a steady-state heat-transfer model, which confirmed the deposition process to be thermally driven. The liquid−deposit interface temperature was found to be equal to WAT of the wax−solvent mixture. The average deposit thermal conductivity was estimated to be 0.35 W m^{-1} K^{-1}.

Experimental results indicated interesting and complex effects of the Reynolds number (or shear rate) and deposition time on the deposit thickness, thermal conductivity, density, composition, and the solid/liquid phase ratio. The results showed that an increase in the Reynolds number (or shear rate) caused an increase in the deposit thermal conductivity, density, and wax content but a decrease in the deposit thickness and its thermal resistance. The deposit thickness, thermal conductivity, density, and wax content increased to their asymptotic values in a deposition time of about 12 h. However, the deposit thermal resistance and the rate of heat transfer were constant over a deposition time of 24 h. These trends were explained in terms of a decrease in the liquid-phase fraction or an increase in the solid-phase fraction in the deposit with an increase in the deposition time.

The GC analysis of deposit samples showed that an increase in the Reynolds number caused an increased wax content, along with an enrichment of heavier *n*-alkanes and a depletion of lighter *n*-alkanes. An increase in the deposition time also caused similar changes in the deposit composition, with the wax content of the deposit increasing to an asymptotic value in about 12 h.

A recently proposed representation, involving one-dimensional deformation of a cubical cage, was used to express the deposit compositional changes in terms of the deformation angle, β. It was found that β increased with both the deposition time and Reynolds number. A viscoplastic model was proposed to describe the changes in the deposit composition, in which β depends upon both the Reynolds number (assumed to be responsible for the initial plastic changes) and the deposition time (assumed to cause the time-dependent viscous changes). A correlation for β was developed that described the observed trends satisfactorily. The model based on the viscoplastic behavior of the deposit is a new approach for explaining the "deposit aging" phenomenon, which in previous studies[11,17] has been interpreted as a time-dependent counter-diffusion process. Overall, the results of this study provide further evidence that the deposition from "waxy" mixtures (or crude oils) is primarily a thermally driven process, in which the deposit properties are influenced by the shear rate and the deposition time.

Acknowledgment. Financial support from the Natural Sciences and Engineering Research Council of Canada (NSERC) and the Department of Chemical and Petroleum Engineering (University of Calgary) is gratefully acknowledged. We thank Mr. Hamid Bidmus, Mr. Nitin Bhat, Mr. Nelson Fong, Ms. Elizabeth Zalewski, Mr. Bernie Then, and Mr. Paul Stanislav for their valuable input, GC analysis, and technical support.

Nomenclature

a = side of the cubical cage (m)
a_1-a_6 = regression constants in eq 6
A_i = inside surface area of deposition tube (m^2)
b_1-b_8 = regression constants in eq 15
C_c = average specific heat capacity of the coolant (J kg^{-1} K^{-1})
C_h = average specific heat capacity of the wax−solvent (hot) mixture (J kg^{-1} K^{-1})
$f(t)$ = a function for the effect of deposition time
h_c = heat-transfer coefficient for the coolant (W m^{-2} K^{-1})
h_h = heat-transfer coefficient for the wax−solvent mixture (W m^{-2} K^{-1})
k_d = average thermal conductivity of the deposit (W m^{-1} K^{-1})
k_m = average thermal conductivity of aluminum (W m^{-1} K^{-1})
L = length of the (aluminum) deposition tube (m)
m_d = mass of the deposit (kg)
$\dot{m}_c$ = mass rate of the coolant (kg s^{-1})
$\dot{m}_h$ = mass rate of the wax−solvent mixture (kg s^{-1})
q = rate of heat transfer at steady state (W)
q_{gain} = rate of heat gain by the coolant from the surroundings, $<0.01q$ (W)
R_c = thermal resistance of the coolant (K W^{-1})
R_d = thermal resistance of the deposit layer (K W^{-1})
R_h = thermal resistance of the wax−solvent mixture (K W^{-1})
R_m = thermal resistance of the (aluminum) deposition tube wall (K W^{-1})
R_{total} = overall thermal resistance (K W^{-1})
Re = Reynolds number
r_i = inside radius of the deposition tube (m)
r_o = outside radius of the deposition tube (m)
t = deposition time (h)
T = temperature (°C or K)
T_c = average temperature of the coolant, $\equiv 0.5(T_{ci} + T_{co})$ (°C)
T_{ci} = inlet temperature of the coolant (°C)
T_{co} = outlet temperature of the coolant (°C)
T_d = liquid−deposit interface temperature (°C)
$T_{d,avg}$ = average deposit temperature, $\equiv 0.5(T_d + T_{wi})$ (°C)
T_h = average temperature of the wax−solvent mixture, $\equiv 0.5(T_{hi} + T_{ho})$ (°C)
T_{hi} = inlet temperature of the wax−solvent mixture (°C)
T_{ho} = outlet temperature of the wax−solvent mixture (°C)
T_L = liquidus temperature (°C)
T_{wi} = inside temperature of the deposition tube (°C)
T_{wo} = outside temperature of the deposition tube (°C)
U_i = overall heat-transfer coefficient based on the inside tube surface area (W m^{-2} K^{-1})
V = volume of the cubical cage (m^3)

V_L = volume fraction of the liquid phase
V_S = volume fraction of the solid phase
V_β = volume of tilted cage at β (m^3)
$V_{L\beta}$ = volume fraction of the liquid phase in the tilted cage
$V_{S\beta}$ = volume fraction of the solid phase in the tilted cage
w_d = mass fraction of C_{20}^+ *n*-alkane in the deposit
W_d = normalized (solvent-free) mass fraction of C_{20}^+ *n*-alkane in the deposit
w_h = mass fraction of C_{20}^+ *n*-alkane in the wax−solvent mixture
W_h = normalized (solvent-free) mass fraction of C_{20}^+ *n*-alkane in the wax−solvent mixture
x_d = deposit-layer thickness (m)
Z = ratio of the thickness of the edge to the side of the cubical cage

Greek Letters
α = empirical constant in eq 7 (kg m^{-3} $°C^{-1}$)
β = deformation angle (deg)
β_o = initial deformation angle at $t = 0$ (deg)
β_∞ = final deformation angle at $t \rightarrow \infty$ (deg)
β_{max} = maximum deformation angle at Re $\rightarrow \infty$ (deg)
ρ_d = density of the deposit (kg m^{-3})
$\rho_{d,avg}$ = density of the deposit at the average deposit temperature (kg m^{-3})
$\rho_{23\ °C}$ = density of the deposit at 23 °C (kg m^{-3})
θ_d = ratio of the deposit (conductive) thermal resistance and total thermal resistance
ξ = edge thickness of the cubical cage (m)

Acronyms
GC = gas chromatography
PPT = pour-point temperature (°C)
WAT = wax appearance temperature (°C)
WDT = wax disappearance temperature (°C)

EF800591P